CHEMISTRY
A EUROPEAN JOURNAL

DOI: 10.1002/chem.200500877

Structural and Magnetic Properties of Mn^{III} and Cu^{II} Tetranuclear Azido Polyoxometalate Complexes: Multifrequency High-Field EPR Spectroscopy of Cu_4 Clusters with $S=1$ and $S=2$ Ground States

Pierre Mialane,*[a] Carole Duboc,*[b] Jérôme Marrot,[a] Eric Rivière,[c] Anne Dolbecq,[a] and Francis Sécheresse[a]

Abstract: Two new azido-bridged polyoxometalate compounds were synthesized in acetonitrile/methanol media and their molecular structures have been determined by X-ray crystallography. The $[\{(\gamma\text{-}SiW_{10}O_{36})Mn_2(OH)_2(N_3)_{0.5}(H_2O)_{0.5}\}_2(\mu\text{-}1,3\text{-}N_3)]^{10-}$ (**1a**) tetranuclear Mn^{III} complex, in which an end-to-end N_3^- ligand acts as a linker between two $[(\gamma\text{-}SiW_{10}O_{36})Mn_2(OH)_2]^{4-}$ units, represents the first manganese–azido polyoxometalate. The magnetic properties have been studied considering the spin Hamiltonian $\mathscr{H}=-J_1(S_1S_2+S_{1*}S_{2*})-J_2(S_1S_{1*})$, showing that antiferromagnetic interactions between the paramagnetic centers ($g=1.98$) occur both through the di-(μ-OH) bridge ($J_1=-25.5\ cm^{-1}$) and the μ-1,3-azido bridge ($J_2=-19.6\ cm^{-1}$). The $[(\gamma\text{-}SiW_{10}O_{36})_2Cu_4(\mu\text{-}1,1,1\text{-}N_3)_2(\mu\text{-}1,1\text{-}N_3)_2]^{12-}$ (**2a**) tetranuclear Cu^{II} complex consists of two $[\gamma\text{-}SiW_{10}O_{36}Cu_2(N_3)_2]^{6-}$ subunits connected through the two μ-1,1,1-azido ligands, the four paramagnetic centers forming a lozenge. The magnetic susceptibility data have been fitted. This reveals ferromagnetic interactions between the four Cu^{II} centers, leading to an $S=2$ ground state ($\mathscr{H}=-J_1(S_1S_2+S_{1*}S_{2*})-J_2(S_2S_{2*})$, $J_1=+294.5\ cm^{-1}$, $J_2=+1.6\ cm^{-1}$, $g=2.085$). The ferromagnetic coupling between the Cu^{II} centers in each subunit is the strongest ever observed either in a polyoxometalate compound or in a di-azido-bridged Cu^{II} complex. Considering complex **2a** and the previously reported basal–basal di-(μ-1,1-N_3)-bridged Cu^{II} complexes in which the metallic centers are not connected by other magnetically coupling ligands, the linear correlation $J_1=2639.5-24.95*\theta_{av}$ between the θ_{av} bridging angle and the J_1 coupling parameter has been proposed. The electronic structure of complex **2a** has also been investigated by using multifrequency high-field electron paramagnetic resonance (HF-EPR) spectroscopy between 95 and 285 GHz. The spin Hamiltonian parameters of the $S=2$ ground state ($D=-0.135(2)\ cm^{-1}$, $E=-0.003(2)\ cm^{-1}$, $g_x=2.290(5)$, $g_y=2.135(10)$, $g_z=2.158(5)$) as well as of the first excited spin state $S=1$ ($D=-0.960(4)\ cm^{-1}$, $E=-0.080(5)\ cm^{-1}$, $g_x=2.042(5)$, $g_y=2.335(5)$, $g_z=2.095(5)$) have been determined, since the energy gap between these two spin states is very small ($1.6\ cm^{-1}$).

Keywords: azides · copper · magnetic properties · manganese · polyoxometalates

Introduction

For several decades, interest in the chemistry of polyoxometalate (POM) compounds has been mainly driven by potential applications in medicine and catalysis, which has led to the search for new structures.[1] More recently, it was shown that POM compounds are also ideal models for the study of exchange interaction in magnetic clusters.[2] To date, complexes containing between one and twenty eight[3] paramagnetic centers embedded in a diamagnetic polyoxotungstate matrix have been reported. While the magnetic exchange interactions have been fully quantified for POM complexes with nuclearities of 2, 3, and 9,[2] and more recently for POM species with nuclearities of 5,[4] 6,[5] and 7,[6]

[a] Dr. P. Mialane, Dr. J. Marrot, Dr. A. Dolbecq, Prof. F. Sécheresse
Laboratoire de Physico-Chimie des Solides Moléculaires
Institut Lavoisier, UMR 8637
Université de Versailles Saint-Quentin
45 Avenue des Etats-Unis, 78035 Versailles Cedex (France)
Fax: (+33) 139-2543-81
E-mail: mialane@chimie.uvsq.fr

[b] Dr. C. Duboc
High Magnetic Field Laboratory of Grenoble
CNRS UPR 5021 BP16, 38042 Grenoble Cedex 9 (France)
Fax: (+33) 4-76-85-56-10
E-mail: duboc@grenoble.cnrs.fr

[c] Dr. E. Rivière
Laboratoire de Chimie Inorganique, UMR 8613
Institut de Chimie Moléculaire et des Matériaux d'Orsay
Université Paris-Sud, 91405 Orsay (France)

among all the magnetic compounds studied, POM complexes containing four paramagnetic centers have been the most widely investigated. Particularly, Dawson- and Keggin-based compounds in which the metal centers M ($M = Mn^{II}$, Fe^{II}, Co^{II}, Ni^{II}, Cu^{II}) are encapsulated by two $\{B\text{-}PW_9O_{34}\}$ or two $\{P_2W_{15}O_{56}\}$ ligands have been synthesized, and their magnetic properties investigated.[7] In these complexes, the magnetic core consists of four edge-sharing $\{MO_6\}$ octahedra forming a well-isolated centrosymmetric rhomb-like $\{M_4O_{16}\}$ unit. Besides this large family of compounds, a POM complex in which a $\{Ni_4O_4\}$ cubane fragment is inserted in a $\{B\text{-}PW_9O_{34}\}$ Keggin unit has been characterized.[8] More recently, two dimeric POM compounds with $\{As^{III}W_9O_{33}\}$ ligands have been reported. In the copper complex, three of the four Cu^{II} centers are adjacent to each other, connected through two μ_3-oxo bridges,[9] while in the Fe^{III} compound, all the iron centers are connected through long O-W-O or O-W-O-W-O bridges.[10] Except for this last compound, in which the metallic centers are nearly magnetically isolated, all the paramagnetic centers are magnetically coupled through oxo or hydroxo bridges. Recently, we have initiated the study of magnetic POM compounds in which the paramagnetic transition-metal ions are connected by azido ligands.[11] For more than two decades, azido-bridged transition-metal complexes have inspired a lot of experimental and theoretical work.[12] It has been established that the end-to-end coordination mode tends to lead to antiferromagnetic coupling, while the end-on coordination generates ferromagnetic coupling. Nevertheless, the absolute value and even the sign of the exchange parameter J are strongly influenced by the coordination mode of the μ-1,1-N_3^- ion, which can bridge either in a symmetrical or an asymmetrical fashion. Indeed, while dinuclear complexes where the azido ligand connects the Cu^{II} centers in a basal–basal end-on fashion (Scheme 1) can be strongly ferromagnetically coupled, the study of related basal–apical systems revealed that the coupling is very weak.[13] This can be easily rationalized considering that the d_{z^2} is a nonmagnetic orbital. Very recently, magnetostructural correlations for such asymmetrically bridged compounds based on DFT calculations have been proposed.[14] Nevertheless, synthesis and physical characterization of new azido-bridged coordination complexes are still of interest to define the structural factors governing the exchange coupling between azido-bridged paramagnetic centers, since magnetostructural correlations have only been proposed for a few systems such as basal–basal end-on Cu^{II}[15] and Mn^{II}[16] compounds. Interestingly, we have shown that the synthesis of POM/N_3^- complexes leads to azido compounds characterized by original structural features that differ from those obtained using organic ligands. Complexes with very large[11] or very small[17] M-(N_3)-M angles have been isolated, as well as a unique Cu^{II} complex in which a μ-1,1,1,3,3,3-azido ligand assembles a nine-paramagnetic-center cluster.[17]

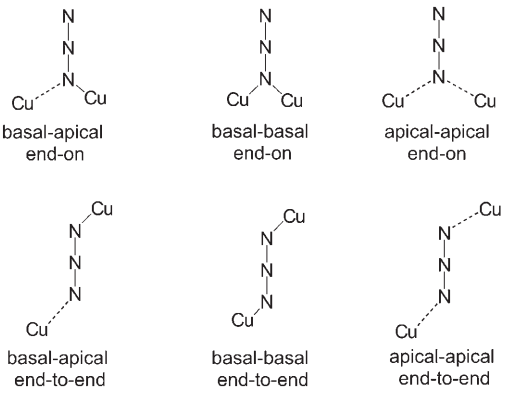

Scheme 1. The six different coordination modes of a bidentate N_3 ligand. The dotted lines indicate long axial Cu–N bonds.

In this paper, we present the synthesis, X-ray crystal structure analysis, and variable-temperature magnetic behavior of two new azido POM compounds with Mn^{III} and Cu^{II} as paramagnetic centers. The high-field electron paramagnetic resonance (HF-EPR) analysis (95–285 GHz) of the Cu^{II} derivative is also reported. The complex $[\{(\gamma\text{-}SiW_{10}O_{36})Mn_2(OH)_2(N_3)_{0.5}(H_2O)_{0.5}\}_2(\mu\text{-}1,3\text{-}N_3)]^{10-}$ (**1a**), in which an end-to-end N_3^- ligand acts as a linker between two $[(\gamma\text{-}SiW_{10}O_{36})Mn_2(OH)_2]^{4-}$ units, represents the first manganese azido POM. The second complex, $[(\gamma\text{-}SiW_{10}O_{36})_2Cu_4(\mu\text{-}1,1,1\text{-}N_3)_2(\mu\text{-}1,1,1\text{-}N_3)_2]^{12-}$ (**2a**) is made up of two $[\gamma\text{-}SiW_{10}O_{36}Cu_2(N_3)_2]^{6-}$ subunits connected by two μ-1,1,1-azido ligands. The ferromagnetic coupling occurring between the Cu^{II} centers in each subunit is the strongest ever observed either in a POM compound or in a diazido-bridged Cu^{II} complex. A correlation between the bridging angle and the coupling parameter for basal–basal di-(μ-1,1-N_3) symmetrically bridged complexes in which the metallic centers are not connected by other magnetically coupling bridges is proposed. Finally, we report the electronic parameters of complex **2a** and of the previously reported $KNaCs_{10}[\gamma\text{-}SiW_{10}O_{36}Cu_2(H_2O)(N_3)_2]_2{\cdot}26H_2O$[17] (**2b**) compound, determined by a multifrequency HF-EPR study, and the results are compared and discussed.

Results and Discussion

Synthesis: Complexes **1a** and **2a** were synthesized at room temperature in acetonitrile/methanol media by mixing the divacant $[N(C_4H_9)_4]_4H_4[\gamma\text{-}SiW_{10}O_{36}]$ precursor[18] with two equivalents of the transition-metal acetate salt and an excess of NaN_3. In both cases, a relatively abundant powder was obtained after addition of tetraethylammonium bromide. Single crystals of compounds **1a** and **2a** were obtained from the filtrate. Elemental analysis, IR, and HF-EPR spectra of the powders have shown that their compositions differ from those of the crystals of complexes **1a** and **2a**, respectively. While we have recently reported Cu^{II}–azido POM compounds synthesized in water, to date it has not been possible to isolate manganese–azido POM compounds under such conditions. In the case of complex **1a**, an X-band EPR spectroscopy analysis of a crystalline sample revealed the pres-

ence of a Mn^{II} impurity, quantified by SQUID measurements as 4% per mole of the whole sample. The systematic presence of such an impurity can be due to the reduction of the Mn^{III} complex by methanol during the crystallization process.

Description of the structures

$[N(C_2H_5)_4]_6[N(C_4H_9)_4]_2H_2[\{(\gamma\text{-}SiW_{10}O_{36})Mn_2(OH)_2(N_3)_{0.5}(H_2O)_{0.5}\}_2(\mu\text{-}1,3\text{-}N_3)]\cdot 15\,H_2O\cdot 4\,CH_3OH$ ***(1a)***: Complex **1a** can be described as a dimer consisting of two $[(\gamma\text{-}SiW_{10}O_{36})Mn_2(OH)_2]^{4-}$ subunits connected through an end-to-end azido ligand (Figure 1a). The structure of the subunits is analogous to that found in the complex $[N(C_6H_5)(CH_3)_3]_4[(SiW_{10}O_{36}Mn_2(OH)_2(H_2O)_2]\cdot H_2O\cdot 2\,CH_3CN$ (**1b**) previously described by Pope and co-workers.[19] In both cases, the two Mn^{III} ions are doubly hydroxo-bridged, the bond-valence sums[20] of the two oxygen atoms bridging the Mn^{III} centers in complex **1a** being 1.03 and 1.01. The Mn···Mn distances are similar in complexes **1a** and **1b** (2.952(4) and 2.934 Å, respectively). Nevertheless, the Mn-O(H)-Mn angles are significantly lower in complex **1a** (88.8(6) and 94.8(5)°) than in **1b** (97.29 and 100.14°), as a consequence of longer Mn–O(H) distances in complex **1a** (d_{Mn-OH} = 1.993(11)–2.125(12) Å). Each Mn^{III} center is in a highly distorted octahedral environment, with four equatorial Mn–O bond lengths ranging from 1.824(10) to 2.125(12) Å and a long axial Mn–O(Si) bond ($d_{Mn-O(Si)}$ = 2.337(7) and 2.359(6) Å). The coordination sphere of the Mn(1) center is completed by a nitrogen atom of the μ-1,3-azido ligand, that connects the two subunits. The Mn(1)–N distance (Figure 1b) is slightly shorter ($d_{Mn(1)-N}$ = 2.227(7) Å) than those previously determined for compounds containing the $\{Mn^{III}(\mu\text{-}1,3\text{-}N_3)Mn^{III}\}$ fragment, the reported Mn–N distances being in the range 2.245(2)–2.349(2) Å.[21] A disorder has been found on the sixth position of the Mn(2) atom, which can be occupied either by a terminal azido ligand or by a water molecule, with equal site occupation factors. However, for steric reasons, complex **1a** cannot accommodate two terminal azido ligands. Thus, the paramagnetic core of complex **1a** can only be described as $\{Mn_4(N_3)(\mu\text{-}1,3\text{-}N_3)(H_2O)\}$. Finally, a strong hydrogen bond between the nonbonded nitrogen atom of the azido ligand and the terminal water molecule connected to the Mn(2) center is observed ($d_{N\cdots O}$ = 2.487(1) Å, Figure 1b).

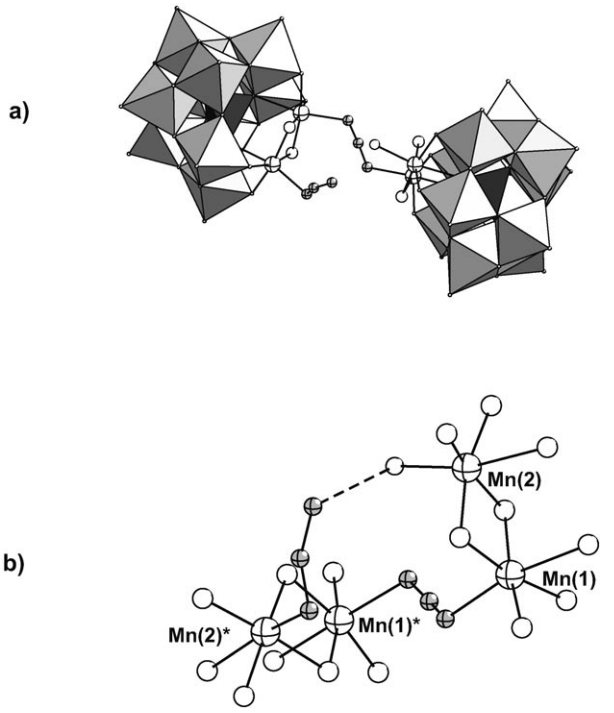

Figure 1. a) Polyhedral and ball-and-stick representations of complex **1a**. b) Ball-and-stick representation of the tetranuclear Mn^{III} fragment in **1a**. The dotted line refers to the $(N_2)N\cdots H(OH)$ hydrogen bond. Light-gray octahedra, WO_6; black octahedra, SiO_4; white, crosshatched spheres, Mn; white spheres, O; gray, crosshatched spheres, N. The stars refer to symmetry-related atoms.

$[N(C_2H_5)_4]_6[N(C_4H_9)_4]_2H_4[(\gamma\text{-}SiW_{10}O_{36})_2Cu_4(\mu\text{-}1,1,1\text{-}N_3)_2(\mu\text{-}1,1,1\text{-}N_3)_2]\cdot 12\,H_2O$ ***(2a)***: The structure can be described as a dimer of $[\gamma\text{-}SiW_{10}O_{36}Cu_2(N_3)_2]^{6-}$ subunits, the connection being through two μ-1,1,1-azido ligands (Figure 2a). Each subunit contains the $[\gamma\text{-}SiW_{10}O_{36}]^{8-}$ polyoxotungstate coordinated to two Cu^{II} centers, bridged by two basal–basal end-on azido groups (d_{Cu-N} = 1.917(13)–2.000(18) Å). The equatorial plane of each Cu^{II} ion is completed by two terminal oxygen atoms of the $[\gamma\text{-}SiW_{10}O_{36}]^{8-}$ subunit (d_{Cu-O} = 1.909(11)–1.974(11) Å). One apical position of each paramagnetic center is occupied by an oxygen atom of the $\{SiO_4\}$ group, with Cu–O(Si) distances of 2.419(11) and 2.606(10) Å. The Cu(1) center (Figure 2b) is then in an axially distorted square-pyramidal environment, while a nitrogen atom of a μ-1,1,1-N_3^- ligand completes the coordination sphere of the Cu(2) center (d_{Cu-N} = 2.602(13) Å), leading to an axially distorted octahedral environment. This explains the much longer Cu–O(Si) distance found for Cu(2) relative to that found for Cu(1), while for compound **1a** the two Mn–O(Si) distances are similar for the two octahedral Mn^{III} centers. The connection through the two μ-1,1,1-azido ligands allows the formation of a tetranuclear Cu^{II} complex. The copper centers form a lozenge of edge-lengths defined by the Cu(1)···Cu(2) and Cu(1)*···Cu(2) distances ($d_{Cu(1)\cdots Cu(2)}$ = 2.875(3) Å and $d_{Cu(1)^*\cdots Cu(2)}$ = 3.439(3) Å). Such a μ-1,1,1-coordination mode remains rare in copper–azido chemistry.[22] The topology of the $\{Cu_2(\mu\text{-}1,1\text{-}N_3)_2\}$ core found in complex **2a** can be compared to that found in the tetranuclear linear complex $KNaCs_{10}[\gamma\text{-}SiW_{10}O_{36}Cu_2(H_2O)(N_3)_2]_2\cdot 26\,H_2O$ (**2b**, Figure 2c) that we recently reported.[17] The arrangement of the Cu_4 cluster is different for these two complexes, as are the Cu(1)-N-Cu(2) angles, which are very important in magnetostructural considerations (see below). The average Cu(1)-N-Cu(2) angle is significantly smaller in complex **2a** (θ_{av} = 94.55°) than in **2b** (θ_{av} = 96.71°). More generally, the θ_{av} angle in complex **2a** is

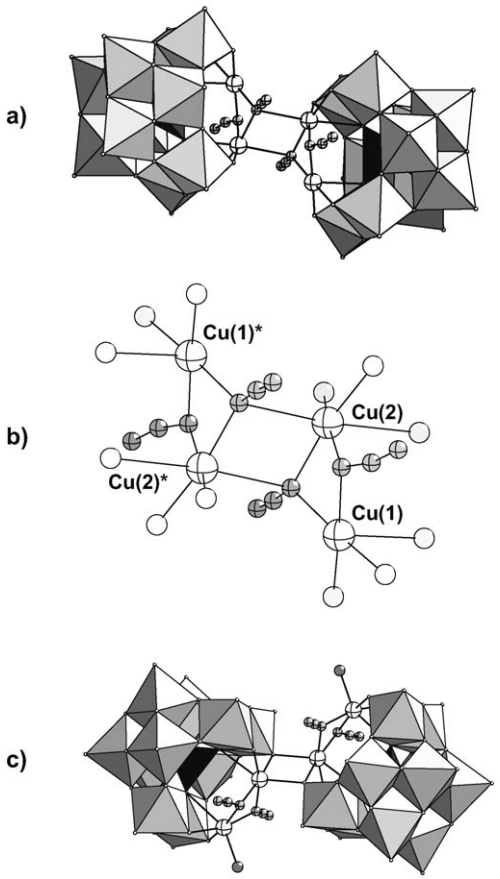

Figure 2. a) Polyhedral and ball-and-stick representations of complex **2a**. b) Ball-and-stick representation of the tetranuclear Cu^{II} fragment in **2a**. c) Polyhedral and ball-and-stick representations of the tetranuclear Cu^{II} fragment in **2b** (reproduced from reference [17]). Light-gray octahedra, WO_6; black octahedra, SiO_4; white, crosshatched spheres, Cu; white spheres, O; gray, crosshatched spheres, N. The stars refer to symmetry-related atoms.

the lowest ever observed in a basal–basal, end-on diazido-bridged copper complex.[23] However, we can mention that a basal–apical, end-on diazido-bridged complex with a θ_{av} angle of 89.1° has been recently reported.[24] Finally, the shortest intermolecular Cu···Cu distance in complex **2a** is very long ($d_{Cu\cdots Cu}=11.877(4)$ Å), implying that the Cu_4 magnetic clusters are well-isolated.

IR spectroscopy: Despite the presence of two distinct azido ligands per molecular unit, the IR spectrum of complex **1a** shows the presence of a single strong band in the 2000–2100 cm^{-1} range; this band was assigned to the asymmetric stretching vibration of the azido ligands ($\nu_{as}=2050\ cm^{-1}$). It has been proposed that the position of the ν_{as} is correlated to the difference between the two N–N distances ($\Delta d'$) of the azido group.[13] In complex **1a**, the $\Delta d'$ values are 0.00 and 0.01 for the bridging and the terminal azido ligands, respectively, suggesting that their respective ν_{as} bands must appear at similar wave numbers ($\nu_{as}\approx 2050\ cm^{-1}$). It should also be noted that Mn^{III} complexes with terminal[25] or bridging azido ligands[21] exhibiting stretching vibrations with very similar wave numbers have been previously reported. For complex **2a**, a strong and relatively broad asymmetric stretching vibration was observed at 2080 cm^{-1}, with a shoulder at 2050 cm^{-1} ($\Delta d'=0.11$ and 0.14 for the μ-1,1- and μ-1,1,1-azido ligands, respectively). A symmetric stretching vibration was observed at 1293 cm^{-1} as a medium band, confirming the presence of asymmetric azido ligands.

Magnetic properties of $[N(C_2H_5)_4]_6[N(C_4H_9)_4]_2H_2[\{(\gamma\text{-}SiW_{10}O_{36})Mn_2(OH)_2(N_3)_{0.5}(H_2O)_{0.5}\}_2(\mu\text{-}1,3\text{-}N_3)]\cdot 15H_2O\cdot 4CH_3OH$ (1a): The magnetic behavior of compound **1a** in the 2–300 K temperature range, corrected assuming 4% per mole of Mn^{II} impurities, is shown in Figure 3 as a $\chi_M T$ against T plot, with χ_M being the magnetic susceptibility for

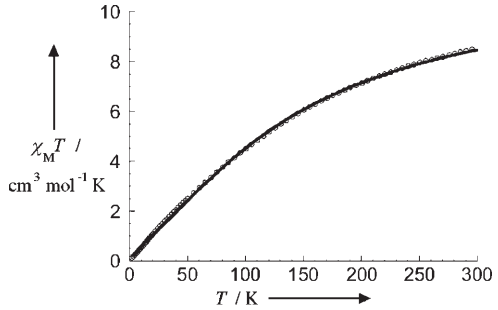

Figure 3. χT per mole of compound **1a** as a function of temperature between 300 and 2 K. The solid line was generated from the best-fit parameters given in the text.

1 mole of complex **1a**. At room temperature, $\chi_M T$ is equal to 8.54 $cm^3 mol^{-1}$ K, a much lower value than what is expected for four uncoupled high-spin Mn^{III} centers ($\chi_M T=12\ cm^3 mol^{-1}$ K assuming $g=2.0$). The $\chi_M T=f(T)$ curve continuously decreased upon sample cooling, reaching a $\chi_M T$ value of 0.11 $cm^3 mol^{-1}$ K at 2 K. This behavior is characteristic of an antiferromagnetic interaction with a diamagnetic ground state. The appropriate Hamiltonian for a linear $\{Mn_4\}$ cluster can be written as Equation (1) in which $S_1=S_2=S_{1*}=S_{2*}=2$.

$$\mathscr{H} = -J_1(S_1S_2 + S_{1*}S_{2*}) - J_2(S_1S_{1*}) \quad (1)$$

The best fitting parameters obtained from the $\chi_M T=f(T)$ curve are $J_1=-25.5\ cm^{-1}$, $J_2=-19.6\ cm^{-1}$ and $g=1.98$ ($R=1.0\times 10^{-5}$),[26] assuming $g=g_{Mn(1)}=g_{Mn(2)}$. While a large number of dibridged Mn^{III} dimers have been reported,[27] only very few Mn^{III} complexes with a $\{Mn(OH)_2Mn\}$ core have been structurally and magnetically characterized. The determined J_1 value is much lower than that observed for the di-μ-oxo-Mn^{III} species ($J=-172.8$ and $-201.4\ cm^{-1}$),[28] confirming the nature of the hydroxo bridges. Moreover, the magnitude of J_1 is in good agreement with the exchange parameter found for complex **1b** ($J_{1b}=-34\ cm^{-1}$, $g=1.965$).[19] Due to the lack of compounds available for comparison, it is difficult to justify the slightly lower value of J_1 compared to that found for **1b**. We can note that this lower J_1 value coin-

cides with a lower θ_{av} angle ($\theta_{av}=91.8$ and 98.7° for complexes **1a** and **1b**, respectively).

Very few end-to-end azido-bridged Mn^{III} complexes have been synthesized,[21d] and to the best of our knowledge magnetic data have only been reported for the structurally characterized $[Mn(salpn)N_3]$[21a,b] ($H_2salpn = N,N'$-bis(salicylidene)-1,3-diaminopropane), $[Mn(salen)N_3]$[21c] ($H_2salen = N,N'$-bis(salicylidene)-1,2-diaminoethane), and $[Mn(acac)_2N_3]$[21c,e] (acac = acetylacetonate) one-dimensional polymeric compounds. The exchange parameters were found to be −8.6, −10.8, and −11.6 cm^{-1}, respectively.[29] The weakness of the σ-type superexchange pathway occurring through the d_{z^2} orbitals in these axially end-to-end azido-bridged Mn^{III} compounds can be attributed to the Jahn–Teller elongation, which leads to long Mn–N(N_2) distances, and then to the weakening of the axial overlap. It therefore seems consistent that the smallest exchange parameter corresponds to the longest Mn–N average distance ($d_{Mn-N}=2.331(4)$ and 2.348(4) Å, $J=-8.6$ cm^{-1} for complex $[Mn(salpn)N_3]$), while the highest J_2 value found for compound **1a** corresponds to the shortest Mn–N distance ($d_{Mn-N}=2.208(7)$ Å, $J_2=-19.6$ cm^{-1}).

Magnetic properties of $[N(C_2H_5)_4]_6[N(C_4H_9)_4]_2H_4[(\gamma\text{-}SiW_{10}O_{36})_2Cu_4(\mu\text{-}1,1,1\text{-}N_3)_2(\mu\text{-}1,1\text{-}N_3)_2]\cdot 12H_2O$ (2a): The magnetic behavior of compound **2a** in the 2–300 K temperature range is shown in Figure 4 as a $\chi_M T$ versus T plot, with χ_M being the magnetic susceptibility for 1 mole of compound **2a**. At room temperature the $\chi_M T$ product is equal to 2.04 $cm^3 mol^{-1} K$, a value already higher than that expected for four uncoupled Cu^{II} centers ($\chi_M T=1.65$ $cm^3 mol^{-1} K$ assuming $g=2.1$). Thus the $\chi_M T$ product increases upon sample-cooling to reach a plateau in the range 70–35 K, and then increases upon sample-cooling to 2 K ($\chi_M T=2.47$ $cm^3 mol^{-1} K$). This is characteristic of a system exhibiting ferromagnetic interactions, with at least two exchange parameters, one being very large and the other relatively small. The appropriate Hamiltonian for the lozenge-shaped cluster **2a** may be written as Equation (2) in which $S_1=S_2=S_{1*}=S_{2*}=1/2$.

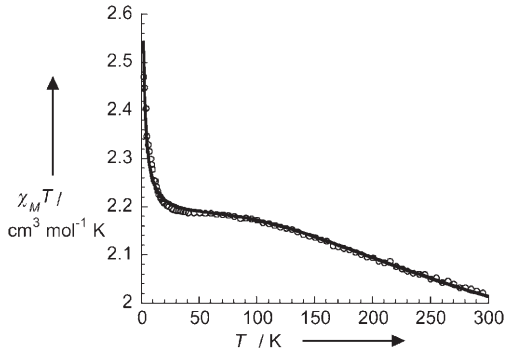

Figure 4. χT per mole of compound **2a** as a function of temperature between 300 and 2 K. The solid line was generated from the best-fit parameters given in the text.

$$\mathscr{H} = -J_1(S_1S_2 + S_{1*}S_{2*}) - J_2(S_2S_{2*}) - J_3(S_1S_{2*} + S_{1*}S_2) \qquad (2)$$

To avoid overparameterization, we have first neglected the last term of the Hamiltonian $\mathscr{H}$ ($J_3=0$), since J_3 reflects the magnetic exchange through one apical–basal, end-on azido ligand between two Cu^{II} centers separated by 3.815(3) Å. The best fitting parameters obtained from the $\chi_M T=f(T)$ curve are $J_1=+294.5$ cm^{-1}, $J_2=+1.6$ cm^{-1} and $g=2.085$ ($R=3.1\times10^{-5}$),[26] assuming $g=g_{Cu(1)}=g_{Cu(2)}$. No improvement has been observed by introducing the J_3 parameter. The J_1 value is the largest ever determined for polyoxometalate complexes, but also for any diazido-bridged Cu^{II} complexes. This result can be understood in light of the studies by Thompson and co-workers on dinuclear, basal–basal, symmetrically bridged μ-1,1-azido complexes,[15] in which the Cu^{II} centers are also connected with a second bridge (μ-hydroxo, μ-1,1-azido, or μ-diazino). For these compounds, the exchange coupling constant increases from approximately −920 cm^{-1} for a Cu-N_3-Cu angle of 123° to +170 cm^{-1} for an angle of 100°. Then, our result is not surprising as complex **2a** exhibits the lowest θ_{av} angle ($\theta_{av}=94.55°$) for this family of compounds. Using the linear correlation proposed by Thompson and co-workers [Eq. (3)], a calculated J_1 value of +477 cm^{-1} is found.

$$J_1 = -41.94\,\theta_{av} + 4440\ cm^{-1} \qquad (3)$$

Considering the discrepancy between the experimental and calculated values, we have listed the structurally and magnetically characterized basal–basal, di-(μ-1,1-N_3) symmetrically bridged complexes previously reported in which the metallic centers are not connected by other efficient magnetically coupling bridges (Table 1). Figure 5 shows the plot $J=f(\theta_{av})$ ($94.55<\theta_{av}<104.7°$) for these complexes and compound **2a**. A good linear fit can be obtained ($R=0.98$),[30] leading to the Equation (4) and to a calculated J_1

Table 1. Cu-N_3-Cu angle [°] and exchange-magnetic-coupling constant J [cm^{-1}] in basal–basal di-μ-1,1-azido-bridged copper(II) complexes.

Complex[a]	θ [θ_{av}]	J	Ref.
$[Cu(tbz)(\mu\text{-}N_3)_2]_2(CH_3OH)_2$	104.7 [104.7][b]	+23	[23d]
$[Cu_2([24]\text{-ane-}N_2O_6)(\mu\text{-}N_3)_4(N_3)_2]\cdot H_2O$	105.5, 101.6 [103.5]	+70	[23b]
$[Cu_2(4\text{-}t\text{Bupy})_4(\mu\text{-}N_3)_2](ClO_4)_2$	100.5 [100.5]	+105	[23a]
$[Cu_2(dmptd)(\mu\text{-}N_3)_2(N_3)_2]$	98.3, 101.9 [100.1]	+170	[23c]
$[Cu_4L^{dur}(\mu\text{-}N_3)_4](PF_6)_4\cdot 4H_2O\cdot 6CH_3CN$	96.6, 98.1 [97.4]	+188	[23e]
2b	96.6, 96.9 [96.7]	+224	[17]
2a	92.6, 96.5 [94.5]	+295	this work

[a] tbz = bis(2-benzimidazolyl)propane; dmptd = 2,5-bis[(pyridylmethyl)thio]thiadiazole; L^{dur} = 1,2,4,5-tetrakis-(1,4,7-triazacyclonon-1-ylmethyl)benzene; tBupy = *ter*-butylpyridin; [24]-ane-N_2O_6 = 1,4,7,13,16,19-hexaoxa-10,22-diazacyclotetracosane. [b] Average values are given between square brackets.

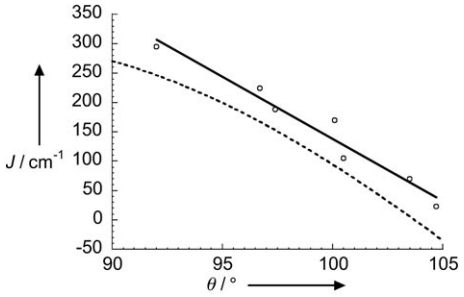

Figure 5. Plot of J versus θ_{av} (average Cu-N-Cu angle) for compound **2a** and its reported congeners (see Table 1). The straight line is the best-linear-fit to the experimental values (see text). The dashed line represents the curve obtained by DFT B3LYP calculations (adapted from reference [31]).

value of 280.5 cm^{-1} for compound **2a**.

$$J_1 = (2639.5 - 24.95\,\theta_{av})\ cm^{-1} \quad (4)$$

Similarly, the related experimental exchange parameter for **2b** ($J_{exptl} = +224\ cm^{-1}$) is also in much better agreement with the calculated value from Equation (4) ($J_{calcd} = +227\ cm^{-1}$) than from Equation (3) ($J_{calcd} = +384\ cm^{-1}$). Moreover, this correlation is in very good agreement with that proposed by Ruiz and co-workers based on DFT B3LYP calculations (Figure 5).[31] Finally, considering Equation (4), the $|J_{AF}| = |J_F|$ situation is expected at $\theta_{av} = 105.8°$.

The J_2 positive value indicates that the two {Cu(1)Cu(2)} and {Cu(1*)Cu(2*)} $S = 1$ pairs are ferromagnetically coupled at low temperature, leading to a quintet ground state. The small absolute value can be easily understood, considering that the exchanged pathway occurs through the nonmagnetic d_{z^2} orbitals, with a very long Cu–N distance ($d_{Cu-N} = 2.602(13)$ Å). To date, only two polymeric μ-1,1,1-azido-bridged compounds have been reported,[22] and even if several asymmetric, end-on azido-bridged complexes have been described, the literature data indicate a dispersion of the J values with regard to Cu-N-Cu angles.[32] Then, it follows that the exchange coupling constant values cannot be rationalized considering only the average bridging angles. Very recently, Triki and co-workers showed that the main parameter controlling the magnetic interaction for asymmetric, end-on azido-bridged complexes is the value of the longest Cu–$N(N_2)$ bond length. Based on DFT calculation, it was found that there is a reduction of the antiferromagnetic coupling when the Cu–$N(N_2)$ bond length increases.[14] However, they proposed that for end-on asymmetrically bridged complexes, the magnetic coupling remains antiferromagnetic whatever the Cu–$N(N_2)$ bond length is. This result seems to be in disagreement with the positive J_2 value determined for complex **2a**. Nevertheless, this suggests that it is difficult to compare the end-on magnetic interactions occurring in asymmetrically μ-1,1,-, μ-1,1,1,-, and μ-1,1,3-azido-dibridged compounds. Finally, we note that ferromagnetic coupling has been previously found for asymmetrically bridged end-on complexes.[33]

Multifrequency HF-EPR experiments

*HF-EPR spectra of $KNaCs_{10}[\gamma\text{-}SiW_{10}O_{36}Cu_2(H_2O)(N_3)_2]_2{\cdot}26H_2O$ (**2b**)*: We first analyzed the HF-EPR spectra of complex **2b**, since the only spin state that contributes to the spectra is the ground spin state $S = 1$.[17] Powder EPR spectra of complex **2b** were recorded between 95 and 285 GHz in a temperature range of 5–30 K. Figure 6 displays

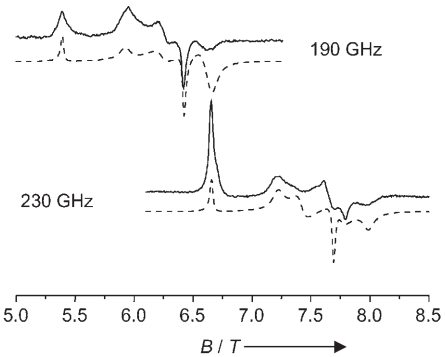

Figure 6. Experimental (——) and simulated (-----) powder HF-EPR spectra of complex **2b** at 15 K recorded at 190 (top) and 230 GHz (bottom). The parameters used for the simulations are given in the text.

the 190 and 230 GHz EPR spectra at 15 K. The triplet spectrum extends from 5.2–7.0 T and from 7.0–8.5 T at 190 and 230 GHz, respectively. The shapes of the EPR spectra are insensitive to temperature. More precisely, upon increasing the temperature from 5 to 30 K, the relative intensity of the different features remains unchanged and only a decrease of the whole spectrum intensity is observed. This implies that the magnitude of D is small compared to the frequencies used in this study ($|D| < 3.3\ cm^{-1}$, 95 GHz). However, since the total width of the overall $S = 1$ spectrum recorded at 190 GHz is close to 2 T, the magnitude of D is smaller than 1 cm^{-1}, implying that the 190 and 230 GHz EPR spectra have been recorded in high-field limit conditions ($D \ll h\nu$) at which the zero-field-splitting (ZFS) parameters are independent of the field.

Thanks to the multifrequency EPR approach, the g value of each transition has been determined from its field evolution as a function of frequency. This allows us to evidence the pairs ($|1,-1> \rightarrow |1,0>$ and $|1,0> \rightarrow |1,1>$ transitions) from the same magnetic axis (6.65 and 7.66 T with $g = 2.30$; 7.22 and 7.98 T with $g = 2.16$; 7.45 and 7.81 T with $g = 2.15$ at 230 GHz). We assign each pair to one magnetic axis by using the field difference ($|\Delta B|_q$ with $q = x$, y, or z) between both transitions. We use the fact that $|\Delta B|_z > |\Delta B|_y > |\Delta B|_x$ if both D and E are positive or negative (with $3|\Delta B|_q = |D|_q/\mu_B g_q$ and $D_x + D_y + D_z = 0$),[34] leading to $g_x = 2.15$, $g_y = 2.16$, and $g_z = 2.30$. The magnitude of D (0.51 cm^{-1}) and E (0.063 cm^{-1}) can be estimated from Equations (5) and (6).

$$|D| = |\Delta B|_z^{*} \mu_B g_z / 2 \quad (5)$$

$$|E| = (|\Delta B|_y{}^*\mu_B g_y - |\Delta B|_x{}^*\mu_B g_x)/6 \quad (6)$$

Accurate determination of the spin Hamiltonian parameters is obtained from simulations of the HF-EPR spectra using a full-matrix diagonalization procedure of the Hamiltonian [Eq. (7)].

$$\mathscr{H}_s = \mu_B B \cdot \mathbf{g} \cdot S + D[S_z^{2-} - 1/3S(S+1)] + E(S_x^2 - S_y^2) \quad (7)$$

Remarkably, EPR spectra at all frequencies can be reproduced with a unique set of parameters ($D = -0.550(2)$ cm^{-1}, $E = -0.065(2)$ cm^{-1}, $|E/D| = 0.118$, $g_x = 2.140(15)$, $g_y = 2.158(4)$, and $g_z = 2.294(3)$). In Figure 6, the simulations of the 190 and 230 GHz EPR spectra are given, and a good agreement between the experimental and simulated spectra is found. The spectra calculated with a negative D fitted the data much better than those calculated with a positive D, deciding the sign of the axial ZFS parameter.

*HF-EPR spectra of $[N(C_2H_5)_4]_6[N(C_4H_9)_4]_2H_4[(\gamma\text{-}SiW_{10}O_{36})_2Cu_4(\mu\text{-}1,1,1\text{-}N_3)_2(\mu\text{-}1,1\text{-}N_3)_2]\cdot 12\,H_2O$ (**2a**)*: In the case of complex **2a**, the ground spin state is $S = 2$ due to the ferromagnetic coupling between two ferromagnetic Cu^{II} dimers. The first excited spin state is a triplet state separated from the ground state by an energy gap of 1.6 cm^{-1}. A singlet is present at 2.4 cm^{-1} and the other spin states are separated from the $S = 2$ spin state by an energy greater than 290 cm^{-1}. Transitions originating from the $S = 2$ and $S = 1$ spin states thus contribute to the EPR spectrum of **2a**. Powder HF-EPR spectra of complex **2a** were recorded between 95 and 285 GHz in a temperature range of 5–30 K. A 190 GHz EPR spectrum recorded at 15 K is shown in Figure 7 with transitions between 5.1 and 7.8 T. As for **2b**, the temperature has no effect on the relative intensity of the EPR transitions, also implying that the high-field-limit conditions are met.

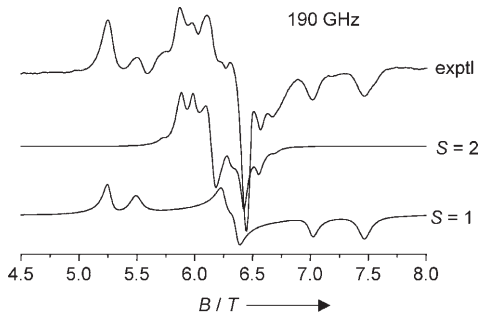

Figure 7. Experimental (exptl) powder 190 GHz HF-EPR spectrum of complex **2a** recorded at 15 K and simulated spectra of the $S = 1$ and $S = 2$ spin states. The parameters used for the simulations are given in the text.

From the shape of the total spectrum shown in Figure 7, two kinds of transition can be distinguished: 1) those at the high- and low-field sides (5.24, 5.49, 7.00, and 7.47 T) are associated with the triplet spin state, and 2) most of those located in the central part (between 6.0 and 6.8 T) are associated with the quintet spin state (two remaining lines from the triplet state are also in the central part).

From the field-dependence of the triplet transitions as a function of frequency, their g value has been calculated. The 5.49 and 7.47 T features appear to issue from the same magnetic direction z with $g = 2.09$. From their field difference (1.98 T), $|D|$ is estimated to be 0.90 cm^{-1} [Eq. (5)]. The $|E|$ term has been estimated to be 0.08 cm^{-1} from Equation (6) with the x and y transitions (the x transitions are located at 6.24 and 7.00 T with $g_x = 2.05$ and $|\Delta B|_x = 0.76$ T, and the y transitions are located at 5.24 and 6.38 T with $g_y = 2.34$ and $|\Delta B|_y = 1.14$ T).

With these estimated values, full diagonalization of the spin Hamiltonian described in Equation (7) gives the parameters $D_1 = -0.960(4)$ cm^{-1}, $E_1 = -0.080(5)$ cm^{-1}, $|E_1/D_1| = 0.083$, $g_{x1} = 2.042(5)$, $g_{y1} = 2.335(5)$, and $g_{z1} = 2.095(5)$ for the $S = 1$ spin state.

As to the transitions originating from the ground spin state $S = 2$, the same analysis gave the following parameters: $D_2 = -0.135(2)$ cm^{-1}, $E_2 = -0.003(2)$ cm^{-1}, $|E_2/D_2| = 0.022$, $g_{x2} = 2.290(5)$, $g_{y2} = 2.135(10)$, and $g_{z2} = 2.158(5)$. Simulated spectra corresponding to the triplet and quintet spin states are shown in Figure 7.

Simulated spectra corresponding to the addition of the quintet and triplet spin states with a 1:1 ratio calculated at 190, 230, and 285 GHz for a temperature of 15 K are shown in Figure 8. We do not consider J here, because the multifrequency EPR investigation shows no other effects that could be related to exchange interaction. The simulations reproduce the field location and the shape of the experimental transitions very well. Good agreement between the relative intensity of the experimental and the simulated features is also obtained. However, the hyperfine structure due to the $Cu^{63,65}$ nuclei was neglected in the simulation. This explains the small intensity differences between the experimental and simulated spectra.

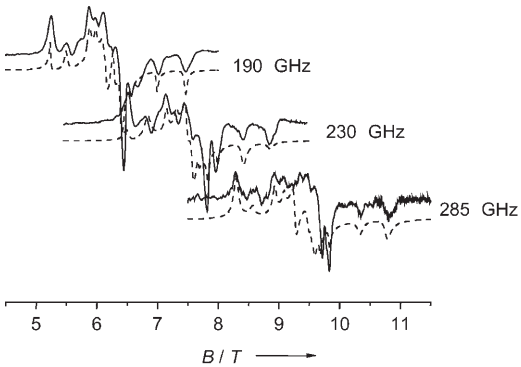

Figure 8. Experimental (——) and simulated (-----) powder HF-EPR spectra of complex **2a** at 15 K recorded at 190 (top), 230 (middle), and 285 GHz (bottom). The parameters used for the simulations are given in the text.

The g values found for complexes **2a** and **2b** are in the range of values expected for Cu^{II} systems. No mononuclear

Cu^{II} complex with similar symmetry and coordination spheres such as in **2a** or **2b** has ever been isolated, so there is no available relation between the *g* values of each copper site and that of the tetramer. This prevents us checking the values found here.

In complex **2b**, the *g* values are different for the triplet and quintet states. However, in previously reported tetranuclear Cu^{II} complexes possessing at least one triplet and one quintet, the *g* values were similar for both states.[35] In these particular cases, the four copper ions have identical ligands and symmetry. In our case, however, each Cu^{II} within a pair is characterized by different symmetries, square-pyramidal for Cu(1) and axially distorted-octahedral for Cu(2). As a consequence, the simplified hypotheses made in previous works based on the symmetry of the complexes cannot apply here. It is then not surprising to find rhombic character and different *g* values for the two spin states. Furthermore, in another Cu^{II} tetramer complex in which the copper ions are not identical, different *g* values were also found for the $S=1$ and $S=2$ states.[9]

The fourth-rank terms of the ZFS were not taken into account in our analysis. The range of *D* values for Cu^{II} clusters (di, tri, or tetranuclear complexes) is very broad and no correlation has been found until now between this parameter and any of the structural properties of the copper complexes (ligand field strength of the ligands, geometry of the copper, coordination number of the metal, and so forth). It can only be noted that the *D* values found for both complexes (**2a**; $D=-0.960\ cm^{-1}$ and **2b**; $D_1=-0.550\ cm^{-1}$) are among the largest for polynuclear copper complexes. For tetranuclear complexes characterized by an S_4 symmetry, the relation $D_1=3D_2$ can be deduced from the known equations linking the ZFS tensors of the different spin states to the six pair interactions of such systems.[35] Here the $|D_1/D_2|$ ratio is about seven for complex **2a**. The low symmetry of complex **2a** certainly implies that the tensors involved are not collinear. This would explain the difference between previous correlations found for high-symmetry systems and our experimental results.

In polynuclear copper(II) complexes, the origin of the ZFS terms is the anisotropic dipolar interaction between the copper ions. This includes the true dipolar magnetic interaction and the pseudodipolar magnetic interaction, also named anisotropic exchange interaction. Since the relative orientations of the tensors of both interactions are unknown, the contribution of each interaction cannot be determined. Crystal HF-EPR measurements would be required for such analysis. Actually, the largest available crystals are still too small to be measured. Finally, it is not relevant to correlate the *E*/*D* ratio with the local symmetry within complexes, since there are many contributions to *E*/*D* arising from the dipolar coupling within each copper pair and between the pairs.

Conclusion

This report demonstrates that the use of vacant POM complexes as ligands leads to azido magnetic complexes with topologies different from those obtained using organic ligands. We can also note that syntheses performed in organic media lead to complexes in which the magnetic cluster arrangement differs from that isolated in aqueous media. Complexes **2a** and **2b** represent the two di-μ-1,1-N_3 symmetrically bridged Cu^{II} species with the smallest bridging angles, and therefore the largest ferromagnetic exchange parameters ever observed for di-μ-1,1-N_3–Cu^{II} complexes, but also for all the previously reported POM compounds. Furthermore, the four Cu^{II} ions are not identical. This results in a low symmetry for these compounds and peculiar electronic properties, such as *g* values with rhombic character. For both complexes, the magnitude of *D* of the triplet, available through HF-EPR measurements only, lies remarkably among the largest expected for such polynuclear systems. Our successful HF-EPR investigation demonstrates that these new compounds provide excellent opportunities for exploring electronic properties of low-symmetry tetranuclear complexes. In the future, single-crystal experiments are planned in order to properly define the directions of the different tensors, a necessary step towards determination of the electronic parameters of each Cu^{II} ion.

On the other hand, complex **1a**, which contains both a terminal and a bridging azido ligand, represents a very rare example of a molecular azido-bridged Mn^{III} complex.[21d] Moreover, it has been shown that nitridomanganese(v) species can be obtained by photooxidation of azido–manganese(III) compounds.[36] It follows that complex **1a** is a good precursor for the synthesis of a POM complex containing the Mn≡N group, which can potentially act as a nitrogen-atom-transfer reagent to substrates such as olefins.[37] We are currently working on the isolation of azido complexes of higher nuclearity, with trivacant POM complexes in place of the $[\gamma\text{-}SiW_{10}O_{36}]^{8-}$ precursor used in this study and in our previous report.[17] We are also extending our investigations to other paramagnetic transition metals.

Experimental Section

Chemicals and reagents: All chemicals were used as purchased without purification. $[N(C_4H_9)_4]_4H_4[\gamma\text{-}SiW_{10}O_{36}]$[18] and $KNaCs_{10}[\gamma\text{-}SiW_{10}O_{36}Cu_2(H_2O)(N_3)_2]_2\cdot 26H_2O$[17] (**2b**) were synthesized as previously described.

Synthesis of $[N(C_2H_5)_4]_6[N(C_4H_9)_4]_2H_2[\{(\gamma\text{-}SiW_{10}O_{36})Mn_2(OH)_2(N_3)_{0.5}O_{36})Mn_2(OH)_2(N_3)_{0.5}(H_2O)_{0.5}\}_2(\mu\text{-}1,3\text{-}N_3)]\cdot 15H_2O\cdot 4CH_3OH$, (1a): $Mn(CH_3COO)_3\cdot 2H_2O$ (78 mg, 0.291 mmol) in methanol (2 mL) was added to $(N(C_4H_9)_4)_4H_4[\gamma\text{-}SiW_{10}O_{36}]$ (500 mg, 0.146 mmol) dissolved in acetonitrile (2 mL). Then, NaN_3 (38 mg, 0.585 mmol) in methanol (2 mL) was added. The solution was stirred for 1 h, and tetraethylammonium bromide (200 mg, 0.952 mmol) was added. The resulting precipitate was filtered off, and the filtrate was allowed to stand in a closed crystallization dish for three days. After filtration, dark-brown crystals of **1a** suitable for single-crystal X-ray diffraction were collected. Yield: 90 mg (18%); IR (KBr pellets): $\tilde{\nu}=2050$ (s), 1632 (m), 1484(s), 1455 (m), 1437 (m), 1393 (m), 1173 (m), 1053 (m), 1000 (m), 954 (s), 911 (s), 896 (s), 867 (s), 788

(s), 750 (m), 695 (s), 553 (m), 535 (m), 485 (w), 392 (m), 355 (m), 306 cm^{-1} (m); elemental analysis calcd (%) for $Si_2W_{20}Mn_4C_{84}H_{246}N_{14}O_{96}$ (6941.7): W 52.97, Mn 3.17, C 14.53, H 3.57, N 2.82; found: W 52.82, Mn 3.10, C 14.48, H 3.26, N 2.86.

Synthesis of $(N(C_2H_5)_4)_6(N(C_4H_9)_4)_2H_4[(\gamma\text{-}SiW_{10}O_{36})_2Cu_4(\mu\text{-}1,1,1\text{-}N_3)_2(\mu\text{-}1,1,1\text{-}N_3)_2]\cdot 12H_2O$ (2a): $Cu(CH_3COO)_2$ (106 mg, 0.584 mmol) in methanol (8 mL) was added to $(N(C_4H_9)_4)_4H_4[\gamma\text{-}SiW_{10}O_{36}]$ (1 g, 0.293 mmol) dissolved in acetonitrile (4 mL). NaN_3 (56 mg, 0.861 mmol) in methanol (6 mL) was added dropwise, and the solution was stirred for 1 h. Then, tetraethylammonium bromide (800 mg, 3.808 mmol) was added, and the resulting suspension was stirred for 20 min. The precipitate was filtered off and the filtrate was allowed to stand in a closed crystallization dish for 3 h. After filtration, green crystals of **2a** suitable for X-ray diffraction were collected. Yield: 360 mg (36%); IR (KBr pellets): $\tilde{\nu}$ = 2080 (s), 2050 (sh), 1630 (m), 1484 (s), 1456 (m), 1439 (m), 1392 (m), 1293 (m), 1172 (m), 1002 (m), 955 (s), 908 (s), 896 (s), 869 (s), 770 (s), 723 (m), 555 (m), 536 (m), 410 (w), 400 (w), 357 (m), 303 cm^{-1} (w); elemental analysis calcd (%) for $Si_2W_{20}Cu_4C_{80}H_{220}N_{20}O_{84}$ (9793.9): W 54.12, Cu 3.74, C 14.14, H 3.26, N 4.12; found: W 54.04, Cu 3.61, C 14.13, H 3.12, N 4.00.

X-ray crystallography: Intensity data collections for compounds **1a** and **2b** were carried out with a Bruker Nonius X8 APEX2 diffractometer equipped with a CCD detector by using $Mo_{K\alpha}$-monochromatized radiation (λ = 0.71073 Å). Due to their instability toward air, single crystals of both complexes were mounted on a glass fiber in Paratone-N oil and intensity data collections were performed at 100 K. The absorption corrections were based on multiple and symmetry-equivalent reflections in the data set using the SADABS program based on the method of Blessing.[38] The structures were solved by direct methods and refined by the full-matrix least-squares method by using the SHELX-TL package.[39] For complex **1a**, the data set was corrected for disordered tetraalkylammonium counterions with the program PLATON/SQUEEZE.[40] Crystallographic data are given in Table 2. Selected bond lengths are listed in Table 3. CCDC-278832 and CCDC-278833 contain the supplementary crystallographic data for compounds **1a** and **2a**, respectively. These data can be obtained free of charge from the Cambridge Crystallographic Data Centre via www.ccdc.cam.ac.uk/data_request/cif.

Table 2. Crystallographic data for $[N(C_2H_5)_4]_6[N(C_4H_9)_4]_2H_2[\{(\gamma\text{-}SiW_{10}O_{36})Mn_2(OH)_2(N_3)_{0.5}(H_2O)_{0.5}\}_2(\mu\text{-}1,3\text{-}N_3)]\cdot 15H_2O\cdot 4CH_3OH$ (**1a**) and $[N(C_2H_5)_4]_6[N(C_4H_9)_4]_2H_4[(\gamma\text{-}SiW_{10}O_{36})_2Cu_4(\mu\text{-}1,1,1\text{-}N_3)_2(\mu\text{-}1,1\text{-}N_3)_2]\cdot 12H_2O$ (**2a**).

	1a	**2a**
empirical formula	$Si_2W_{20}Mn_4C_{84}H_{246}N_{14}O_{96}$	$Si_2W_{20}Cu_4C_{80}H_{220}N_{20}O_{84}$
M_r	6941.7	6793.9
crystal system	monoclinic	monoclinic
space group	*C*2/*c* (No. 15)	*P*2(1)/*n* (No. 14)
a [Å]	19.3013(15)	14.4787(14)
b [Å]	22.0978(16)	14.4905(16)
c [Å]	41.725(3)	37.755(4)
β [°]	97.657(4)	97.252(4)
V [Å^3]	17638(2)	7858(1)
Z	4	2
ρ_{calcd} [g cm^{-3}]	2.616	2.871
μ [mm^{-1}]	13.363	15.208
T [K]	100(2)	100(2)
data/parameters	15528/510	8153/592
R [$>2\sigma(I)$]	$R_1(F_o)^{[a]} = 0.0683$	$R_1(F_o)^{[a]} = 0.0762$
	$wR_2(F_o^2)^{[b]} = 0.2128$	$wR_2(F_o^2)^{[b]} = 0.1861$
R (all data)	$R_1(F_o)^{[a]} = 0.0913$	$R_1(F_o)^{[a]} = 0.1307$
	$wR_2(F_o^2)^{[b]} = 0.2245$	$wR_2(F_o^2)^{[b]} = 0.2239$

[a] $R_1 = \Sigma\,|F_o| - |F_c|\,/\Sigma\,|F_c|$. [b] $wR_2 = \{\Sigma[w(F_o^2 - F_c^2)^2]/\Sigma[w(F_o^2)^2]\}^{1/2}$.

Table 3. Selected bond lengths [Å] and angles [°] for $[N(C_2H_5)_4]_6[N(C_4H_9)_4]_2H_2[\{(\gamma\text{-}SiW_{10}O_{36})Mn_2(OH)_2(N_3)_{0.5}(H_2O)_{0.5}\}_2(\mu\text{-}1,3\text{-}N_3)]\cdot 15H_2O\cdot 4CH_3OH$ (**1a**) and $[N(C_2H_5)_4]_6[N(C_4H_9)_4]_2H_4[(\gamma\text{-}SiW_{10}O_{36})_2Cu_4(\mu\text{-}1,1,1\text{-}N_3)_2(\mu\text{-}1,1\text{-}N_3)_2]\cdot 12H_2O$ (**2a**).

	1a	**2a**
W–O_a[b]	2.275(7)–2.358(7) [2.324][a]	2.231(9)–2.360(10) [2.308]
W–$O_{b,c}$[b]	1.719(9)–2.057(14) [1.903]	1.811(11)–2.094(11) [1.917]
W–O_d[b]	1.665(9)–1.767(11) [1.719]	1.663(12)–1.748(10) [1.713]
Si–O	1.582(7)–1.657(16) [1.628]	1.601(10)–1.667(11) [1.639]
M–O_{eq}	1.824(10), 1.907(12), 1.946(12), 1.960(9)	1.909(11), 1.937(10), 1.943(11), 1.974(11)
Mn–O(H)	1.993(11), 2.018(10), 2.094(13), 2.125(12)	
M–O_{Si}	2.337(7), 2.359(6)	2.419(11), 2.606(10)
M–N_{ax}	2.210(15), 2.227(17)	2.602(13)
Cu–N_{eq}		1.917(13), 1.937(13), 1.979(18), 2.000(18)
Mn-O(H)-Mn	88.8(6)–94.8(5)	
Cu-N_{eq}-Cu		92.6(7)–96.5(6)

[a] Average values are given between square brackets. [b] O_a refers to the oxygen atoms bound to the silicon atom, $O_{b,c}$ to the W-O-W bridging oxygen atoms, and O_d to the terminal W=O terminal oxygen atom.

Magnetic measurements: Magnetic susceptibility measurements were carried out with a Quantum Design SQUID Magnetometer with an applied field of 1000 G by using powder samples pressed into pellets to avoid preferential orientation of the crystallites. The independence of the susceptibility value with regard to the applied field was checked at room temperature. The susceptibility data were corrected from the diamagnetic contributions as deduced by using Pascal's constant tables. The $\chi T = f(T)$ curve related to compound **1a** has been corrected assuming 4% of Mn^{II} monomeric impurities. The presence of this impurity has been confirmed by X-band EPR spectroscopy.

Elemental analysis: Elemental analyses were performed by the Service Central d'Analyse of CNRS, 69390 Vernaison, France.

Infrared spectra: Infrared spectra were recorded from samples as KBr pellets on an FTIR Nicolet 550 apparatus.

X-band EPR spectroscopy: Spectra were recorded on a Bruker ELEXSYS 500 spectrometer.

Multifrequency HF-EPR studies: Studies were performed on a custom-built spectrometer[41] by using powder samples pressed into pellets to avoid preferential orientation of the crystallites in the strong magnetic field. Gunn diodes operating at 95 and 115 GHz and equipped with a second- and third-harmonic generator were used as the radiation source. The magnetic field was produced by a superconducting magnet (0–12 T). We used a temperature regulation apparatus between 4 K and room temperature. Measurements were performed under nonsaturated conditions.

Acknowledgements

We thank the Transnational Access to Infrastructure–Specific Support Action Program (contract no. RITA-CT-2003-505474) of the European Commission.

[1] a) M. T. Pope, *Heteropoly and Isopoly Oxometalates*, Springer, Berlin, **1983**; b) *Polyoxometalate Chemistry for Nanocomposite Design* (Eds.: T. Yamase, M. T. Pope), Kluwer, Dordrecht, The Netherlands, **2002**; c) "Polyoxometalates": *Chem. Rev.* **1998**, *98*, 1–390; d) R. Contant, G. Hervé, *Rev. Inorg. Chem.* **2002**, *22*, 63.

[2] J. M. Clemente-Juan, E. Coronado, *Coord. Chem. Rev.* **1999**, *193–195*, 361.

[3] B. Godin, Y.-G. Chen, J. Vaissermann, L. Ruhlmann, M. Verdaguer, P. Gouzerh, *Angew. Chem.* **2005**, *117*, 3132; *Angew. Chem. Int. Ed.* **2005**, *44*, 3072.
[4] L.-H. Bi, U. Kortz, *Inorg. Chem.* **2004**, *43*, 7961.
[5] L.-H. Bi, U. Kortz, S. Nellutla, A. C. Stowe, J. van Tol, N. S. Dalal, B. Keita, L. Nadjo, *Inorg. Chem.* **2005**, *44*, 896.
[6] J. M. Clemente-Juan, E. Coronado, A. Forment-Aliaga, J. R. Galán-Mascarós, C. Giménez-Saiz, C. J. Gómez-García, *Inorg. Chem.* **2004**, *43*, 2689.
[7] a) T. J. R. Weakley, H. T. Evans, Jr., J. S. Showell, *J. Chem. Soc. Chem. Commun.* **1973**, 139; b) R. G. Finke, M. W. Droege, P. J. Domaille, *Inorg. Chem.* **1987**, *26*, 3886; c) T. J. R. Weakley, R. G. Finke, *Inorg. Chem.* **1990**, *29*, 1235; d) C. J. Gómez-García, E. Coronado, P. Gómez-Romero, N. Casañ-Pastor, *Inorg. Chem.* **1993**, *32*, 3378; e) C. J. Gómez-García, J. J. Borrás-Almenar, E. Coronado, L. Ouahab, *Inorg. Chem.* **1994**, *33*, 4016; f) C. J. Gómez-García, E. Coronado, L. Ouahab, *Angew. Chem.* **1992**, *104*, 660; *Angew. Chem. Int. Ed. Engl.* **1992**, *31*, 649; g) C. J. Gómez-García, E. Coronado, J. J. Borrás-Almenar, *Inorg. Chem.* **1992**, *31*, 1667; h) N. Casañ-Pastor, J. Bas, E. Coronado, G. Pourroy, L. C. W. Baker, *J. Am. Chem. Soc.* **1992**, *114*, 10380; i) H. Andres, J. M. Clemente-Juan, M. Aebersold, H. U. Güdel, E. Coronado, H. Büttner, G. Kearly, J. Melero, R. Burriel, *J. Am. Chem. Soc.* **1999**, *121*, 10028; j) J. M. Clemente-Juan, H. Andres, M. Aebersold, J. J. Borrás-Almenar, E. Coronado, H. U. Güdel, H. Büttner, G. Kearly, *Inorg. Chem.* **1997**, *36*, 2244; k) J. M. Clemente-Juan, H. Andres, J. J. Borrás-Almenar, E. Coronado, H. U. Güdel, M. Aebersold, G. Kearly, H. Büttner, M. J. Zolliker, *J. Am. Chem. Soc.* **1999**, *121*, 10021.
[8] U. Kortz, A. Tézé, G. Hervé, *Inorg. Chem.* **1999**, *38*, 2038.
[9] U. Kortz, S. Nellutla, A. C. Stowe, N. S. Dalal, J. van Tol, B. S. Bassil, *Inorg. Chem.* **2004**, *43*, 144.
[10] U. Kortz, M. G. Savelieff, B. S. Bassil, B. Keita, L. Nadjo, *Inorg. Chem.* **2002**, *41*, 783.
[11] P. Mialane, A. Dolbecq, E. Rivière, J. Marrot, F. Sécheresse, *Angew. Chem.* **2004**, *116*, 2324; *Angew. Chem. Int. Ed.* **2004**, *43*, 2274.
[12] For a review on Ni^{II}– and Mn^{II}–azido-bridged complexes, see: J. Ribas, A. Escuer, M. Monfort, R. Vicente, R. Cortés, L. Lezama, T. Rojo, *Coord. Chem. Rev.* **1999**, *193–195*, 1027.
[13] M. S. Ray, A. Ghosh, R. Bhattacharya, G. Mukhopadhyay, M. G. B. Drew, J. Ribas, *Dalton Trans.* **2004**, 252.
[14] S. Triki, C. J. Gómez-García, E. Ruiz, J. Sala-Pala, *Inorg. Chem.* **2005**, *44*, 5501.
[15] L. K. Thompson, S. S. Tandon, M. E. Manuel, *Inorg. Chem.* **1995**, *34*, 2356.
[16] T. K. Karmakar, B. K. Ghosh, H.-K. Fun, E. Rivière, T. Mallah, G. Aromi, S. K. Chandra, *Inorg. Chem.* **2005**, *44*, 2391.
[17] P. Mialane, A. Dolbecq, J. Marrot, E. Rivière, F. Sécheresse, *Chem. Eur. J.* **2005**, *11*, 1771.
[18] E. Cadot, V. Béreau, B. Marg, S. Halut, F. Sécheresse, *Inorg. Chem.* **1996**, *35*, 3099.
[19] X.-Y. Zhang, C. J. O'Connor, G. B. Jameson, M. T. Pope, *Inorg. Chem.* **1996**, *35*, 30.
[20] N. E. Brese, M. O'Keeffe, *Acta Crystallogr. Sect. B* **1991**, *47*, 192.
[21] a) K. R. Reddy, M. V. Rajasekharan, J.-P. Tuchagues, *Inorg. Chem.* **1998**, *37*, 5978; b) H. Li, Z. J. Zhong, C.-Y. Duan, X.-Z. You, T. C. W. Mak, B. Wu, *Inorg. Chim. Acta* **1998**, *271*, 99; c) A. Panja, N. Shaikh, P. Vojtíšek, S. Gao, P. Banerjee, *New J. Chem.* **2002**, *26*, 1025; d) N. Hoshino, T. Ito, M. Nihei, H. Oshio, *Inorg. Chem. Commun.* **2003**, *6*, 377; e) R. B. Stults, R. S. Marianelli, V. W. Day, *Inorg. Chem.* **1975**, *14*, 722.
[22] a) L. Zhang, L.-F. Tang, Z.-H. Wang, M. Du, M. Julve, F. Lloret, J. T. Wang, *Inorg. Chem.* **2001**, *40*, 3619; b) M. A. S. Goher, T. C. W. Mak, *Inorg. Chim. Acta* **1985**, *99*, 223.
[23] a) O. Kahn, S. Sikorav, J. Gouteron, S. Jeannin, Y. Jeannin, *Inorg. Chem.* **1984**, *23*, 490; b) J. Comarmond, P. Plumeré, J.-M. Lehn, Y. Agnus, R. Louis, R. Weiss, O. Kahn, I. Morgenstern-Badarau, *J. Am. Chem. Soc.* **1982**, *104*, 6330; c) S. S. Tandon, L. K. Thompson, E. M. Manuel, J. N. Bridson, *Inorg. Chem.* **1994**, *33*, 5555; d) G. A. Van Albada, M. T. Lakin, N. Veldman, A. L. Spek, J. Reedjik, *Inorg. Chem.* **1995**, *34*, 4910; e) B. Graham, T. W. Hearn, P. C. Junk, C. M. Kepert, F. E. Mabbs, B. Moubaraki, K. S. Murray, L. Spiccia, *Inorg. Chem.* **2001**, *40*, 1536.
[24] S. Koner, S. Saha, T. Mallah, K.-I. Okamoto, *Inorg. Chem.* **2004**, *43*, 840.
[25] S. Deoghoria, S. K. Bera, B. Moulton, M. J. Zaworotko, J.-P. Tuchagues, G. Mostafa, T.-H. Lu, S. K. Chandra, *Polyhedron* **2005**, *24*, 343.
[26] $R=[\Sigma(\chi_M T_{calcd}-\chi_M T_{obsd})^2/\Sigma(\chi_M T_{obsd})^2]$.
[27] S. Mukhopadhyay, S. Mandal, S. Bhaduri, W. H. Armstrong, *Chem. Rev.* **2004**, *104*, 3981.
[28] a) P. A. Goodson, A. R. Oki, J. Glerup, D. J. Hodgson, *J. Am. Chem. Soc.* **1990**, *112*, 6248; b) J. Glerup, P. A. Goodson, A. Hazell, R. Hazell, D. J. Hodgson, C. J. McKenzie, K. Michelsen, U. Rychlewska, H. Toftlund, *Inorg. Chem.* **1994**, *33*, 4105.
[29] From reference [21b].
[30] $R=[\Sigma(J_{calcd}-J_{obsd})^2/\Sigma(J_{obsd})^2]$.
[31] E. Ruiz, J. Cano, S. Alvarez, P. Alemany, *J. Am. Chem. Soc.* **1998**, *120*, 11122.
[32] See reference [13] and references therein.
[33] K. Matsumoto, S. Ooi, K. Nakatsura, W. Mori, S. Suzuki, A. Nakahara, Y. Nakao, *J. Chem. Soc. Dalton Trans.* **1985**, 2095.
[34] A. Abragam, B. Bleaney, *Electron Paramagnetic Resonance of Transition Ions*, Dover Publications, New York, **1970**.
[35] a) A. Bencini, D. Gatteschi, C. Aanchini, J. G. Haasnoot, R. Prins, J. Reedijk, *J. Am. Chem. Soc.* **1987**, *109*, 2926; b) A. Bencini, D. Gatteschi, *EPR of Exchange Coupled Systems*, Springer, Berlin (Germany), **1990**; c) E. A. Buvaylo, V. N. Kokozay, O. Y. Vassilyeva, B. W. Skelton, J. Jezierska, L.-C. Brunel, A. Ozarowski, *Inorg. Chem.* **2005**, *44*, 206.
[36] a) P.-K. Chan, C.-K. Poon, *J. Chem. Soc. Dalton Trans.* **1976**, 858; b) K. Meyer, J. Bendix, N. Metzler-Nolte, T. Weyhermüller, K. Wieghardt, *J. Am. Chem. Soc.* **1998**, *120*, 7270.
[37] L. A. Bottomley, F. L. Neely, *J. Am. Chem. Soc.* **1988**, *110*, 6748.
[38] R. Blessing, *Acta Crystallogr. Sect. A* **1995**, *51*, 33.
[39] The structures were solved by direct methods and refined by the full-matrix least-squares method by using the SHELX-TL package: G. M. Sheldrick, SHELX-TL version 6.14, Software Package for Crystal Structure Determination, Siemens Analytical X-ray Instrument Division, Madison, WI USA **2000**.
[40] A. L. Spek, *Acta Crystallogr. Sect. A* **1990**, *46*, C34.
[41] a) A.-L. Barra, J.-C. Brunel, J.-B. Robert, *Chem. Phys. Lett.* **1990**, *165*, 107; b) F. Muller, M. A. Hopkins, N. Coron, M. Grynderg, J.-C. Brunel, G. Martinez, *Rev. Sci. Instrum.* **1989**, *60*, 3681.

Received: July 25, 2005
Published online: January 10, 2006

